Available online at www.sciencedirect.com
ScienceDirect
Physica E 40 (2008) 2263–2267
PHYSICA E
www.elsevier.com/locate/physe

Complex superstructure patterns near defect sites of carbon nanotubes and graphite

L. Tapasztó[a,*], P. Nemes-Incze[a], Z. Osváth[a], M.C. Bein[a], Al. Darabont[b], L.P. Biró[a]

[a]Research Institute for Technical Physics and Materials Science, P.O. Box 49, H-1525 Budapest, Hungary
[b]Faculty of Physics, "Babes-Bolyai" University, Street M. Kogalniceanu No. 1, R-3400 Cluj-Napoca, Romania

Available online 29 September 2007

Abstract

Atomic resolution scanning tunneling microscope (STM) images of native and artificially created defect sites on graphite and carbon nanotubes were compared. The presence of position-dependent coexisting superstructure patterns was identified on all of the investigated samples. The results indicate that superstructure patterns are mainly determined by the available scattered states of the system rather than the detailed structure of the defect site. We propose an interference model, which can explain the presence of coexisting superstructures both on graphite and carbon nanotubes. The model predicts reduced corrugation amplitude for the case of graphite as compared to carbon nanotubes due to the wave-vector averaging on the Fermi circle.

PACS: 73.22.−f

Keywords: Nanotubes; Graphite; Defects; Superstructures; Interference; STM

1. Introduction

Understanding how imperfections influence the electronic behavior of materials is of fundamental importance. In the case of nanostructured materials, defects play an even more accentuated role. When the size of the system becomes comparable to the coherence length of the electrons, quantum mechanical effects become of crucial importance. Scattering processes occurring at defect sites of nanostructures not simply increase the resistance of the sample but the interference of the incident and defect-scattered electrons should also be considered. Carbon nanotubes are famous for their almost perfect structure, however, some defects are still present in their structure [1]. One should be aware of the effects caused by the presence of these defect sites on the electron transport for instance when willing to utilize carbon nanotubes as ballistic interconnects in future molecular electronic devices [2]. On the other hand, artificially introducing defects in the structure of carbon nanotubes is also interesting from the application's point of view. A metallic carbon nanotube acts as a ballistic conductor [3], however, inducing defect sites in its structure may give rise to complex functional devices such as single-electron transistors (SET) operable at room temperature [4]. Therefore, the precise determination of the structure of defects occurring in nanotubes and the detailed understanding of their effects on electronic properties of the sample are of major importance in the development of molecular electronic devices.

Unfortunately, there are very few methods able to provide direct information about the structure of the defects in carbon nanotubes and their influence on the electronic behavior of the tube. Scanning tunneling microscopy (STM) is a method which can provide information both on atomic and local electronic structure of the sample. This makes STM a powerful tool in the investigation of structural defects of carbon nanotubes. However, the advantage of the method raises difficulties in the interpretation of the measurements, since the information concerning the atomic and electronic structure of the sample are mixed together in STM images.

*Corresponding author.
E-mail address: tapaszto@mfa.kfki.hu (L. Tapasztó).

1386-9477/$ - see front matter © 2007 Elsevier B.V. All rights reserved.
doi:10.1016/j.physe.2007.09.122

In order to separate the effects, theoretical efforts have to be done [5].

Several works have reported the STM investigation of defect sites of graphite [6–9] and more recently, carbon nanotubes [10–13]. The atomic resolution images revealed the existence of superstructure patterns near the defect site with a periodicity larger than, but commensurate to the underlying atomic structure. These patterns are known as $\sqrt{3} \times \sqrt{3}R30^{\circ}$-type superstructures [6]. Mizes and Foster [9] demonstrated that the origin of the observed superstructures is the perturbation of electronic structure rather than the rearrangement of the atomic lattice near the defect site. Shedd and Russell [14] proposed a simple and intuitive phenomenological method in order to interpret and reproduce the experimentally observed superstructures as the interference of defect-scattered and regular states of the graphite. Two main interference patterns are predicted by the method, those corresponding to constructive and destructive phase condition between the regular and defect-scattered wave functions. This method predicts only the existence of homogenous superstructures. However, more complex pattern showing the position-dependent coexistence of different types of superstructures was experimentally observed [6,7,14] without a consistent interpretation of these observations. In this paper, we show that the coexistence of different superstructures is a common phenomenon, occurring near different defect types on both graphite surfaces and carbon nanotubes. We propose a theoretical model for both nanotubes and graphite samples, based on the interference method, which is able to reproduce the experimentally observed coexisting superstructures on both systems.

2. Experimental

Different samples were prepared and investigated by STM under ambient conditions.

(1) In order to induce defect sites, the freshly cleaved highly oriented pyrolytic graphite (HOPG) samples were exposed to a heat treatment in air at 600 °C. The exposure time was 5 min. This procedure produced monolayer pits on the graphite surface of diameters between 10 and 40 nm under current experimental conditions. This treatment makes it easier to find suitable sites for measurements since it produces dense well-defined defect sites.

(2) In order to create point-like defects in the HOPG, the samples were irradiated with Ar^+ ions of 30 keV with a dose of 5×10^{11} ion/cm^2. The dose was chosen carefully in order to create individual defects but with a high enough density to be easily found by STM.

(3) Multi-walled carbon nanotubes (MWCNTs) produced by chemical vapor deposition (CVD) methods often contain native structural defects due to the relatively low growth temperature. We have investigated MWCNTs produced by an injection pyrolysis CVD method involving the pyrolysis of a ferrocene/xylene solution. The synthesis process was carried out at 800 °C in Ar atmosphere [15].

(4) MWCNTs produced by electric-arc discharge technique usually contain much less defects than the CVD grown ones due to the elevated synthesis temperatures. In order to artificially create defect sites, the nanotubes deposited on a HOPG substrate were irradiated by Ar^+ with the same parameters as for the irradiated HOPG samples.

In order to carry out STM measurements on nanotubes, 1 mg of the nanotube sample was ultrasonicated in toluene for 60 min, then droplets of this suspension were dispersed on a HOPG substrate.

All the STM measurements were carried out in constant current mode with tunneling currents of 0.3–1 nA and bias voltages in the range of 0.1–1 V. Atomic resolution images were typically achieved with 0.1 V bias voltage and 1 nA tunnel current.

3. Results

Fig. 1a shows the STM image of the HOPG sample exposed to heat treatment at 600 °C for 5 min.

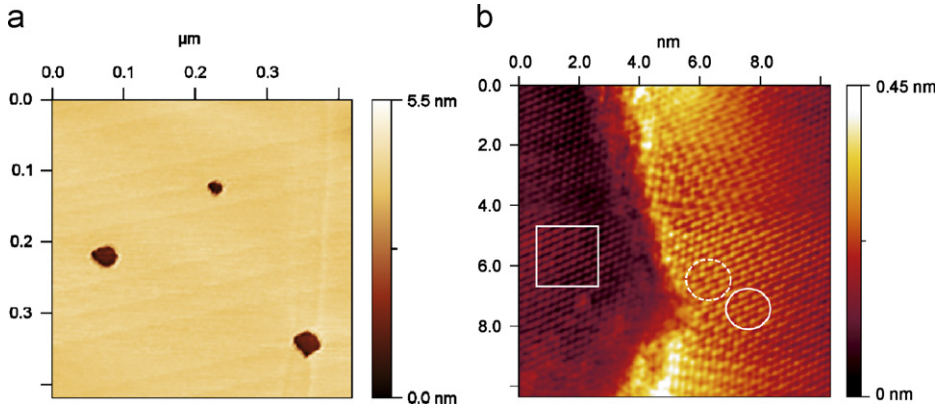

Fig. 1. (a) STM image of one monolayer deep pits on HOPG formed by thermal treatment in air, at 600 °C, for 5 min. (b) Atomic resolution obtained at the edge of a pit. The square marks the normal atomic resolution STM image of graphite on the lower layer. On the defective upper layer, different superstructure patterns are present marked by dashed and solid circles.

The features observed in the image are pits of one monolayer depth with typical diameters in the range of 10–40 nm. The pit chosen for detailed investigation has a diameter of about 30 nm. Along the edge of the pit, we were able to obtain atomic resolution STM images, which revealed superstructure patterns resembling the well-known $\sqrt{3} \times \sqrt{3}R30^{\circ}$-type superstructures of graphite. However, different kinds of these superstructures are present side by side on the atomic resolution STM images. The interference pattern corresponding to constructive interference (full-lined circle) is located in the close vicinity of the pattern attributed to destructive interference of defect-scattered electronic wave functions (broken-lined circle). Atomic resolution could be simultaneously achieved in the defect-free lower graphene layer. The STM images revealed the expected triangular lattice corresponding to the atomic periodicity of the β-carbon atom sites of the HOPG [16].

Fig. 2 shows the STM image of Ar^+ ion-irradiated HOPG surface. The defect sites induced by the impacts of Ar^+ ions are most probably vacancies [17]. However, the dangling bonds of the vacancies might get saturated under ambient conditions.

The typical size of the defects, in this case, is 1 order of magnitude smaller than for the case of heat-treated HOPG sample. The defect sites can be identified as hillock-like protrusions on the STM images. It has been shown that these features are due to the electronic states localized at the defect sites [12]. These additional localized states have energies near the Fermi level, hence can contribute to the tunnel current. In the atomic resolution images taken near these defect sites, coexisting superstructure patterns were identified.

In Fig. 3, we present the STM investigation of a CVD-grown MWCNT with an apparent diameter of about 40 nm. It is well known that due to relatively low synthesis temperatures, defects often occur in the structure of CVD-grown nanotubes. Moving along the axis of the nanotubes during the STM measurements, we were able to identify defective regions. Atomic resolution STM images achieved near a native defect site of the investigated nanotube also displayed the coexistence of different superstructure patterns.

Finally, we have investigated by STM Ar^+ ion-irradiated multi-wall nanotube samples. In accordance with the expectations, the STM images of irradiated

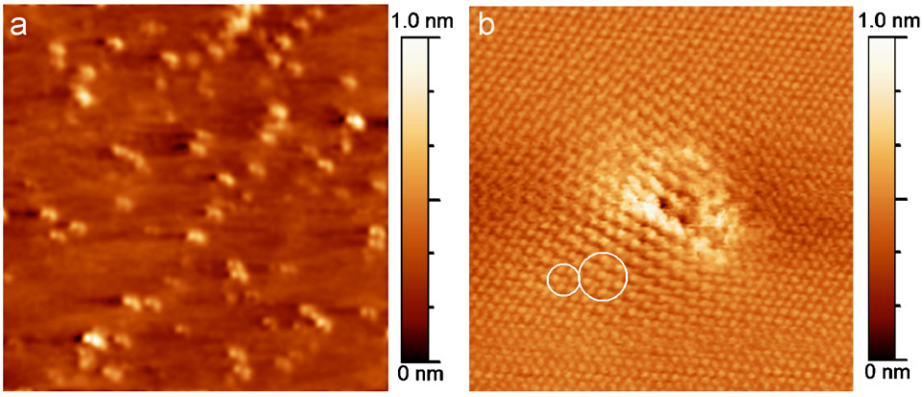

Fig. 2. (a) STM image of ion-irradiated HOPG surface (scan range $100 \times 100\,nm^2$). The defects created by the impact of ions can be observed as hillock-like protrusions. (b) Atomic resolution image near a single-defect site displaying position-dependent superstructure patterns ($10 \times 10\,nm^2$ scan area).

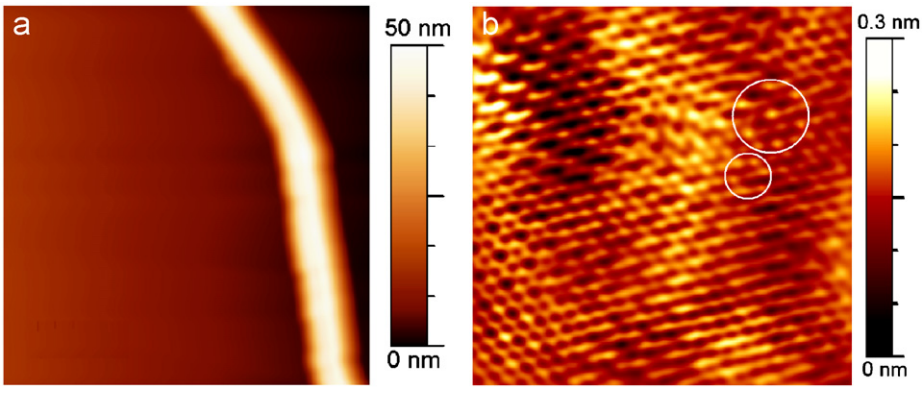

Fig. 3. (a) STM image of a CVD-grown multi-walled carbon nanotube (scan area $200 \times 200\,nm^2$). (b) Atomic resolution image achieved near a defective region of the nanotube ($8 \times 8\,nm^2$).

nanotubes showed the presence of hillock-like protrusions on the walls of the tubes, similarly to the case of ion-irradiated HOPG. Looking at the atomic resolution STM images, we were able to identify again the coexistence of different patterns of electronic superstructures (Fig. 4).

From these results, we can draw the conclusion that the presence of position-dependent coexisting superstructures is quite common near defect sites of graphite and nanotubes. However, theoretical models considering the scattering of the electrons on defects sites which are successful in the interpretation of the homogenous superstructures failed to give an interpretation for the coexisting superstructure patterns. A common characteristic of these models is that for the sake of simplification of the calculations they only consider the scattering of the electrons located exactly at the K points of the Brillouin zone.

We proposed a model, which considers electronic states in the vicinity of the K points to be involved in the scattering processes. This model is schematically presented in Fig. 5.

Several mechanisms can be responsible for the shifting of the Fermi level from the bands crossing points (K points). The most probable is the doping of the sample, i.e. the charge transfer between the sample and impurities attached to it, since the structural defects may act as preferred sites for impurities.

Similar models can be applied for the case of metallic carbon nanotubes and graphite when considering only electronic states at the K points to be involved in the scattering processes. However, when we take into account the shift of the Fermi level form the K points, an important difference arise, namely that in the case of the graphite, all the states corresponding to the equi-energetic Fermi circle get involved in the scattering (see Fig. 5), while for the case of nanotubes, the quantization of the wave vector perpendicular to the axis of the nanotube selects two points (allowed electronic states) of the Fermi circle as we discussed in an earlier work [13]. Now we extend our model to the case of graphite. In this case, the wave function of the electrons involved in the tunneling can be written as a superposition of regular and defect-scattered states of the

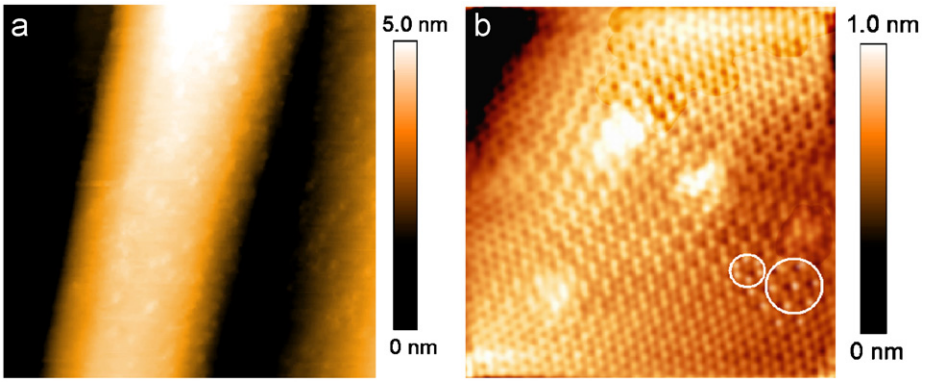

Fig. 4. (a) STM image ($100 \times 100\,nm^2$) of a multi-wall carbon nanaotube irradiated with Ar^+ ions. The defects created by ion can be seen as small protrusions on the outer wall of the nanotubes. (b) Atomic resolution image ($10 \times 10\,nm^2$) observed near defects sites.

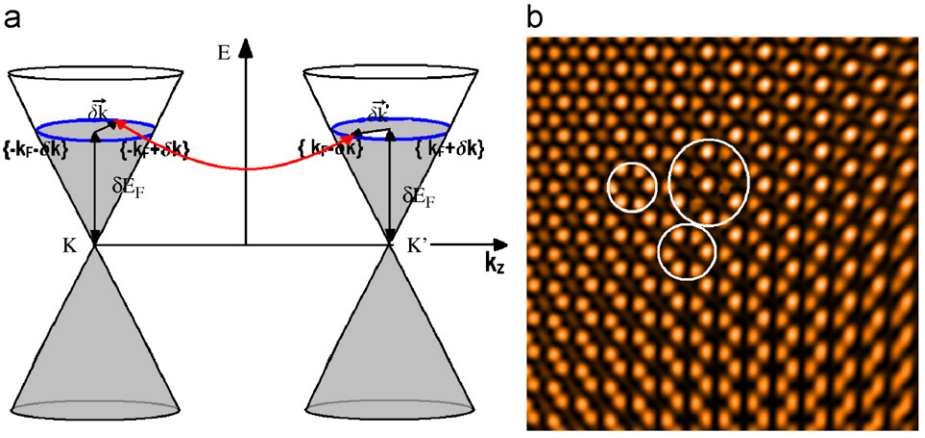

Fig. 5. (a) Possible scattering mechanisms near the bands crossing points of two nonequivalent K points of the Brillouin zone for the case of graphite. (b) Simulated STM image considering the interference of defect-scattered electronic states located on the shifted Fermi circle of the graphite.

graphite considering electronic states on the whole Fermi circles:

$$\Psi(\vec{r}) = \int_{E_F}^{E'_F} \mathrm{d}E \oint_F \delta\vec{k} \oint_{F'} \delta\vec{k}' \sum_{\{\vec{k}_F^j\}} \left(\phi_j \, \mathrm{e}^{\mathrm{i}(\vec{k}_F^j + \delta\vec{k}(E))\cdot\vec{r}} + R_j \, \mathrm{e}^{-\mathrm{i}(\vec{k}_F^j + \delta\overrightarrow{k'}(E))\cdot\vec{r}} \right) \quad (1)$$

where the F and F' are the Fermi circles corresponding to the two nonequivalent points of the first Brillouin zone K and K', respectively. The radius of the Fermi circles is given by: $|\delta\vec{k}(E)| = (2|E_F - E|)/3\gamma_0 a_{C-C}$, where γ_0 is the nearest-neighbor C–C energy overlap integral and a_{C-C} is the nearest neighbor distance between C atoms. The R_j coefficients are reflection amplitudes representing the contribution of different scattered states. Since they are complex numbers, the information regarding the phase shift of the scattered states is included. Using this model, we can reproduce the presence of position-dependent coexisting superstructure patterns for a broad range of the scattering parameters (R_j coefficients) and Fermi level shift, which can explain the ubiquitous presence of these patterns.

Due to the above-mentioned difference for the case of graphite and carbon nanotubes, the model predicts a slight blurring of the superstructure pattern for the case graphite as compared to the nanotubes due to the averaging of the wave-vectors. However, the main feature, the coexistence of superstructures, remains unchanged for both cases.

4. Conclusions

In conclusion, we have compared atomic resolution STM images near different types of defect sites on carbon nanotubes and graphite. The atomic resolution images revealed the presence of coexisting superstructure patterns on all the investigated samples, which suggest that these patterns are quite common. The results also indicate that superstructure patterns are primarily determined by the available scattered states of the system rather than the detailed structure of the defect. We have proposed a theoretical model, which can explain the presence of these superstructures by considering the scattering of electronic wave functions slightly away from the K points of the Brillouin zone. These theoretical results also predict a reduced corrugation of the superstructure patterns for the case of the graphite samples as compared to carbon nanotubes, due to the wave-vector averaging around the Fermi circle. However, for the experimental validation, further investigations are required.

Acknowledgments

This work has been funded by OTKA, Grant no. T 049131 and no. T 049182 and NKTH Grant MOFENACS.

References

[1] Y. Fan, B.R. Goldsmith, P.G. Collins, Nat. Mater. 4 (2005) 906.
[2] M. Bockrath, W. Liang, D. Bozovic, J.H. Hafner, C.M. Lieber, M. Tinkham, H. Park, Science 291 (2001) 283.
[3] C.T. White, T.N. Todorov, Nature 393 (1998) 240.
[4] H.W.C. Postma, T. Teepen, Z. Yao, M. Grifoni, C. Dekker, Science 293 (2001) 76.
[5] W.A. Hofer, A.S. Foster, A.L. Shluger, Rev. Mod. Phys. 75 (2003) 1287.
[6] J. Xhie, K. Sattler, U. Muller, N. Venkateswaran, G. Raina, Phys. Rev. B 43 (1991) 8917.
[7] P. Ruffieux, O. Gröning, P. Scwaller, L. Sclapbach, P. Gröning, Phys. Rev. Lett. 84 (2000) 4910.
[8] P. Ruffieux, M. Melle-Franco, O. Groning, M. Bielmann, F. Zerbetto, P. Groning, Phys. Rev. B 71 (2005) 153403.
[9] H.A. Mizes, J.S. Foster, Science 244 (1989) 559.
[10] W. Clauss, D.J. Bergeron, M. Freitag, C.L. Kane, E.J. Mele, A.T. Johnpson, Eur. Phys. Lett. 47 (1999) 601.
[11] A. Hassanien, M. Tokumoto, P. Umek, D. Mihailovic, A. Mrzel, Appl. Phys. Lett. 78 (2001) 808.
[12] Z. Osváth, G. Vértesy, L. Tapasztó, F. Wéber, Z.E. Horváth, J. Gyulai, L.P. Biró, Phys. Rev. B 72 (2005) 045429.
[13] L. Tapasztó, P. Nemes-Incze, Z. Osváth, A. Darabont, P. Lambin, L.P. Biró, Phys. Rev. B 73 (2006) 235422.
[14] G.M. Shedd, P.E. Russell, Surf. Sci. 266 (1992) 259.
[15] L. Tapasztó, K. Kertész, Z. Vértesy, Z.E. Horváth, A.A. Kóos, Z. Osváth, Z. Sárközi, Al. Darabont, L.P. Biró, Carbon 43 (2005) 790.
[16] D. Tomanek, S.G. Louie, H.J. Mamin, D.W. Abraham, R.E. Thomson, E. Ganz, J. Clarke, Phys. Rev. B 35 (1987) 7790.
[17] A.V. Krasheninnikov, K. Nordlund, M. Sirviö, E. Salonen, J. Keinonen, Phys. Rev. B 63 (2001) 245405.